

Probing the Gravitational Well: No Supernova Explosion in Spherical Symmetry with General Relativistic Boltzmann Neutrino Transport

Matthias Liebendörfer^{1,2,3}, Anthony Mezzacappa², Friedrich-Karl Thielemann^{1,2},
O. E. Bronson Messer^{2,3,4}, W. Raphael Hix^{2,3,4}, Stephen W. Bruenn⁵

¹ *Department of Physics and Astronomy, University of Basel,
Klingelbergstrasse 82, CH-4056 Basel Switzerland*

² *Physics Division, Oak Ridge National Laboratory, Oak Ridge, TN 37831-6354*

³ *Department of Physics and Astronomy, University of Tennessee, Knoxville, TN 37996-1200*

⁴ *Joint Institute for Heavy Ion Research, Oak Ridge National Laboratory,
Oak Ridge, TN 37831-6374*

⁵ *Department of Physics, Florida Atlantic University, Boca Raton, FL 33431-0991*

We report on the stellar core collapse, bounce, and postbounce evolution of a $13 M_{\odot}$ star in a self-consistent general relativistic spherically symmetric simulation based on Boltzmann neutrino transport. We conclude that approximations to exact neutrino transport and omission of general relativistic effects were not alone responsible for the failure of numerous preceding attempts to model supernova explosions in spherical symmetry. Compared to simulations in Newtonian gravity, the general relativistic simulation results in a smaller shock radius. We however argue that the higher neutrino luminosities and rms energies in the general relativistic case could lead to a boost in the explosion energy of an exploding supernova.

I. BACK TO THE PAST?

In the pioneering days of supernova simulations (Colgate and White [1], May and White [2]) the consideration of general relativity (GR) was standard. The observable event of a stellar core collapse followed by a supernova explosion was an ideal application for the newly derived Einstein equations in spherical symmetry (Misner and Sharp [3]). Lindquist [4] formulated the GR Boltzmann equation, and Wilson [5] carried out simulations based on GR Boltzmann neutrino transport with parametrized neutrino interactions. This early epoch laid the foundation leading to our current understanding of the supernova mechanism: A collapsing stellar iron core bounces at nuclear densities and launches a shock wave outwards through the infalling outer layers. The shock is energized by neutrinos diffusing out of the hot proto-neutron star and depositing a fraction of their energy in the shock-dissociated matter via absorption on the free nucleons.

The early models have been refined in many respects. The equation of state evolved from simple polytropes to significantly more realistic models (Baron et al. [6], Lattimer and Swesty [7]). The neutrino opacities were improved (Schinder and Shapiro [8], Bruenn [9], Burrows and Lattimer [10], Mezzacappa and Bruenn [19]), and sophisticated multigroup flux-limited diffusion neutrino transport schemes were developed based on this “standard” nuclear physics input (Arnett [11], Bowers and Wilson [12], Bruenn [9], Myra et al. [13]).

However, improved approximations in the implementation of neutrino physics seemed to decrease the likelihood of successful explosions in spherical symmetry. This was especially true with the full inclusion of the energy spectrum of the neutrinos in multigroup simulations and for simulations that took the inelastic neutrino-electron scattering into account (Bruenn [14,15]). The idea that the amount of dissociation energy expended by the shock ploughing through the outer iron core might be small enough to allow a prompt explosion had to be abandoned. The energy that is deposited behind the shock by the outstreaming neutrinos (Wilson and Mayle [16]) gained increased attention in light of a possible delayed shock revival. The transferred energy, however, does not alone depend on the neutrino spectrum and luminosity of the neutrinos, but also on their angular distribution. The neutrino propagation angle determines the path length in a given radial shell; therefore, neutrinos with more tangential directions have a higher chance of absorption. A known problem of the multigroup flux-limited diffusion approximation to the Boltzmann transport equation is that, just in the important semi-transparent region between the neutrinosphere and the heating region, the angular distribution of the neutrinos is not self-consistently determined by the transport equation. The consequence is an underestimation of the isotropy of the outstreaming neutrinos (Janka [17]).

The focus therefore switched on the one hand to the development of exact three-flavor Boltzmann neutrino transport (Mezzacappa and Bruenn [18–20]) and to stationary comparisons between exact transport and multigroup flux-limited diffusion schemes (Messer et al. [21], Yamada et al. [22]). More efficient heating was found with accurate transport. On the other hand, multidimensional phenomena were explored in the hope to increase the heating efficiency. The inclusion of neutron finger convection (see also Ref. [23]) produced explosions (Wilson and Mayle [16]) and established the delayed explosion scenario. Two-dimensional investigations of convection behind the shock and in the proto-neutron star followed with mixed results (Herant et al. [24], Miller et al. [25], Herant et al. [26], Burrows et al. [27], Janka and Müller [28], Keil et al. [29], Mezzacappa et al. [30,31]). Multi-dimensional simulations with general relativistic effects were performed by Fryer [32] and Fryer and Heger [33].

Semi-analytical investigations (Burrows and Goshy [34], and recently Janka [35]) illuminate the basic mechanisms, but are not able to self-consistently decide for or against explosions nor able to predict detailed data in either of these cases.

In the search for a robust supernova mechanism, attention was directed toward simulations in the nonrelativistic (NR) limit, because explosions in GR seemed to be less likely in the selective picture that the deeper shock formation would produce larger dissociation losses and that the neutrino luminosities would suffer gravitational redshift.

However, there are also beneficial effects: Baron et al. [36] reported prompt explosions in general relativity with a very soft equation of state and a leakage scheme, although these explosions were not reproduced in a general relativistic multigroup flux-limited diffusion simulation by Myra et al. [37] when neutrino electron scattering was included. Swesty

et al. [38] also do not find an explosion in a systematic investigation of realistic parameters in the equation of state. Late time beneficial effects related to the decrease in the gravitational potential by neutrino energy radiation were suggested by Goldman and Nussinov [39]. De Nisco et al. [40], in a quasi-static investigation, pointed out that, among many detrimental effects, the hotter core in general relativistic hydrodynamics produces higher neutrino luminosities with harder spectra, resulting in a potentially beneficial impact on the heating rate. Recent dynamical simulations with GR multigroup flux-limited diffusion confirm this effect, although it does not appear to be strong enough to outweigh the negative GR contributions, i.e. the smaller heating region and greater infall velocities. (Bruenn et al. [41]).

Recently, postbounce evolution was reexamined with Boltzmann neutrino transport apart from invoking multi-dimensional effects. Caused by an undervalued nucleon isoenergetic scattering opacity, first simulations led to an explosion of a $13 M_{\odot}$ progenitor (Liebendörfer [42]). Simulations in Newtonian gravity with $O(v/c)$ Boltzmann transport and standard nuclear physics for the same progenitor do lead to an enhanced shock radius, but not to an explosion (Mezzacappa et al. [43]). Even with the omission of the energy loss due to the escape of μ - and τ neutrinos, independent simulations of the postbounce evolution of a $15 M_{\odot}$ progenitor do not produce an explosion (Rampp and Janka [44]). The latter simulations are based on the tangent-ray method (Burrows et al. [45]) for the $O(v/c)$ Boltzmann neutrino transport.

It is the purpose of this paper to report, after Wilson’s pioneering work [5], on the completion of a general relativistic radiation hydrodynamics code in spherical symmetry to implement a solution to the exact Boltzmann transport equation, and present the self-consistent simulation of stellar core collapse, bounce and postbounce evolution for a $13 M_{\odot}$ star, with all neutrino flavors and standard nuclear physics included.

II. THE RECIPE

Our simulation is initiated from the stellar precollapse model of Nomoto and Hashimoto [46]. We use the Lattimer-Swesty equation of state [7]. Simplified silicon burning is included as material from the silicon layer surrounding the iron core is instantaneously burned under energy conservation to nuclear statistical equilibrium as soon as the temperature exceeds 0.44 MeV (Mezzacappa et al. [43]). The simulations were carried out with a new general relativistic neutrino radiation hydrodynamics code, AGILE-BOLTZTRAN, based on a conservative formulation of GR radiation hydrodynamics in spherical symmetry and comoving coordinates (Liebendörfer et al. [47]).

AGILE is an implicit GR hydrodynamics code using an adaptive grid technique to conservatively implement shift vectors (Liebendörfer and Thielemann [48]). It maximizes, with respect to the number of required grid points, the resolution in regions with large density gradients and allows a smooth propagation of the shock through the outer layers (see graph (a) in Fig. (1-5)). BOLTZTRAN is an implicit three-flavor multigroup Boltzmann neutrino transport solver (Mezzacappa and Bruenn [18–20], Mezzacappa and Messer [49]) that was consistently coupled to AGILE, enabled for adaptive gridding, and extended to GR flows (Liebendörfer [42]). We choose 103 spatial zones, and discretize the neutrino-momentum phase space, as in Mezzacappa et al. [43], with 6-point Gaussian quadrature and 12 neutrino energy groups, ranging from 5 MeV to 300 MeV.

We emphasize at this point that the energy evolution in Lagrangian radiation hydrodynamics obeys the very simple conservation equation

$$\begin{aligned} \frac{\partial}{\partial t} \left[\Gamma \epsilon + \frac{2}{\Gamma + 1} \left(\frac{1}{2} U^2 - \frac{m}{R} \right) + \Gamma J + U H \right] \\ + \frac{\partial}{\partial r} [4\pi R^2 e^{\Phi} U p + 4\pi R^2 e^{\Phi} n (U K + \Gamma H)] = 0. \end{aligned} \quad (1)$$

The variables are defined as in Lindquist [4] with the exception that J , H , and K represent the zeroth, first, and second angular moments of the *specific* radiation energy. The integration of Eq. (1) over the total rest mass in the computational domain provides a check on the conservation of total energy, which can easily be monitored. Energy conservation presents a significant challenge. The cancellation of the gravitational binding energy with the internal energy sets the scale of the total energy, which is two orders of magnitude smaller than either contribution separately and comparable to the 10^{51} erg ($\sim 1\%$ of radiation energy) expected to be deposited in the heating region. Our total energy drift is no more than 5×10^{49} erg in the first 200 ms in which the explosion outcome is decided. Lepton number is conserved to within a fraction of a percent.

III. THE FAILED EXPLOSION OF A $13 M_{\odot}$ STAR

We discuss the evolution of our simulation at five time slices: At bounce, and 1 ms, 10 ms, 100 ms, and 500 ms after bounce. At each time slice we show eight graphs that compare the general relativistic evolution (GR, fat lines) to the nonrelativistic evolution (NR, thin lines). We have already reported on the NR simulation in Mezzacappa et al. [43]. The two runs are synchronized at bounce. The graphs are: (a) the velocity profile and the location of the adaptive grid points (for the GR profiles only); (b) the rest mass density profile; (c) the entropy per baryon profile; (d) the electron fraction profile. The latter three quantities enter the equation of state and determine the composition and state of the local fluid element. For the convenience of interpretation, we additionally show the mass fraction of heavy nuclei, free nucleons, and alpha particles in graph (f). The remaining three graphs are devoted to neutrino radiation quantities: (e) the luminosities; (h) the rms energies; and (g), the mean flux factor defined by the quotient of the neutrino energy flux, H , and the neutrino energy density, J : $F \equiv H/(cJ)$. We also show the energy-averaged neutrinospheres in this plot because they separate the interior diffusion regime, with small flux factors, from the exterior regime, where large flux factors describe increasingly forward-peaked neutrino propagation through semitransparent and free streaming regions. The radiation quantities are given for the electron neutrino and the electron antineutrino separately. The μ and τ neutrinos do not exchange energy with the heating region. Their luminosities and rms energies are shown in later Figures. In our discussion, we follow the general relativistic simulation and apply numbers for the nonrelativistic case in parentheses.

The first prominent difference in the GR and NR simulation appears at bounce in Fig. (1). At this time, the inner core passes maximum compression with a central density of $3.87 \times 10^{14} \text{ g/cm}^3$ (NR: $3.05 \times 10^{14} \text{ g/cm}^3$) as shown in graph (b). The homologous collapse of the causally connected inner core is abruptly halted when the central region reaches nuclear density. The short range nuclear forces suddenly increase the stiffness of the equation of state. A pressure wave emerges from the center and steepens into a shock wave at the border of the inner iron core where it faces the disconnectedly infalling material from the outer iron core. We observe the shock formation in the velocity profile in graph (a) at an enclosed mass of $0.53 M_{\odot}$ (NR: $0.65 M_{\odot}$). The conversion of kinetic energy into internal energy at the shock front becomes apparent in the discontinuity of the entropy profile in graph (c). The additional discontinuity at $\sim 1.2 M_{\odot}$ stems from continued silicon burning by compressional heating in the infalling material. From the composition in graph (f), we know that the shock starts to dissociate the heavy nuclei as they fall in. The shock in the NR case encloses a region of undissociated heavy nuclei at high density. The extent of this region is limited by the phase transition to bulk nuclear matter in the Lattimer-Swesty equation of state. These heavy nuclei are not present in the GR case because the shock is formed at smaller radius, almost coincident with the location of the phase transition. The electron fraction profile in graph (d) exhibits values from 0.499 in the outer layers down to 0.29 (NR: 0.28) in the central region. The lepton fraction is set by neutrino trapping during core collapse (Mezzacappa and Bruenn [20]). Thereafter, smaller changes in the electron fraction are allowed according to an establishing equilibrium between electron- and neutrino capture at constant lepton fraction (Messer [50]). Determined by this equilibrium are the rms energies for the electron neutrinos, as shown in graph (h). The mean flux factor in graph (g) reflects an isotropic distribution in the innermost $0.7 M_{\odot}$ and outwardly directed radiation at the border of the computational domain. The peaks in the luminosity in graph (e) are caused by numerical noise in the large prevailing neutrino energy density. The small flux factor in graph (g) for the electron neutrinos demonstrate that no important energy transfer takes place at this artificial luminosity peak in the shock front.

One millisecond later, in Fig. (2), the shock has moved from the edge of the homologous core to densities $\sim 10^{12} \text{ g/cm}^3$ as shown in graph (b). In graph (f) we observe a region of dissociated material behind the shock. The heavy nuclei still present in the NR simulation between the shock heated matter and bulk nuclear matter have a mass of $0.15 M_{\odot}$. They leave the shock an additional energy $\sim 2 \times 10^{51} \text{ erg}$ with respect to the GR simulation. The NR shock in graph (a) still contains kinetic energy while the GR shock has almost completely turned into an accretion shock. In graph (g) we see that the shock approaches the neutrinospheres. Plotted are the energy-averaged neutrinospheres located in the broad region where neutrinos with different energies emanate from the diffusion regime. As the shock passes this region at about 4ms after bounce, an energetic neutrino burst will be released from the hot shocked material rendering it “neutrino-visible” to the outside world. A rise in the electron neutrino luminosity at the neutrinospheres at this time is manifest in graph (e). A dip in the rms energy profiles of the electron antineutrino in graph (h) at a radius $\sim 11 \text{ km}$ results from the fact that these are two distinct regions producing these neutrinos: the cold compressed center of the star and the hot shocked mantle.

The time slice in Fig. (3) corresponds to 10ms after bounce, after the launch of the neutrino burst. The luminosity peak in graph (e) has already propagated to a radius of 1800km. This is consistent with the time of shock breakout, $t = 10\text{ms} - 1800\text{km}/c \simeq 4\text{ms}$. The propagation of the neutrinos is also visible in their rms energies. In graph (h), the neutrinos from collapse, with rms energies $\sim 10\text{MeV}$, are replaced with the burst neutrinos having an rms energy of almost 15MeV . The electron neutrinos in the burst were produced by electron capture on free protons. The

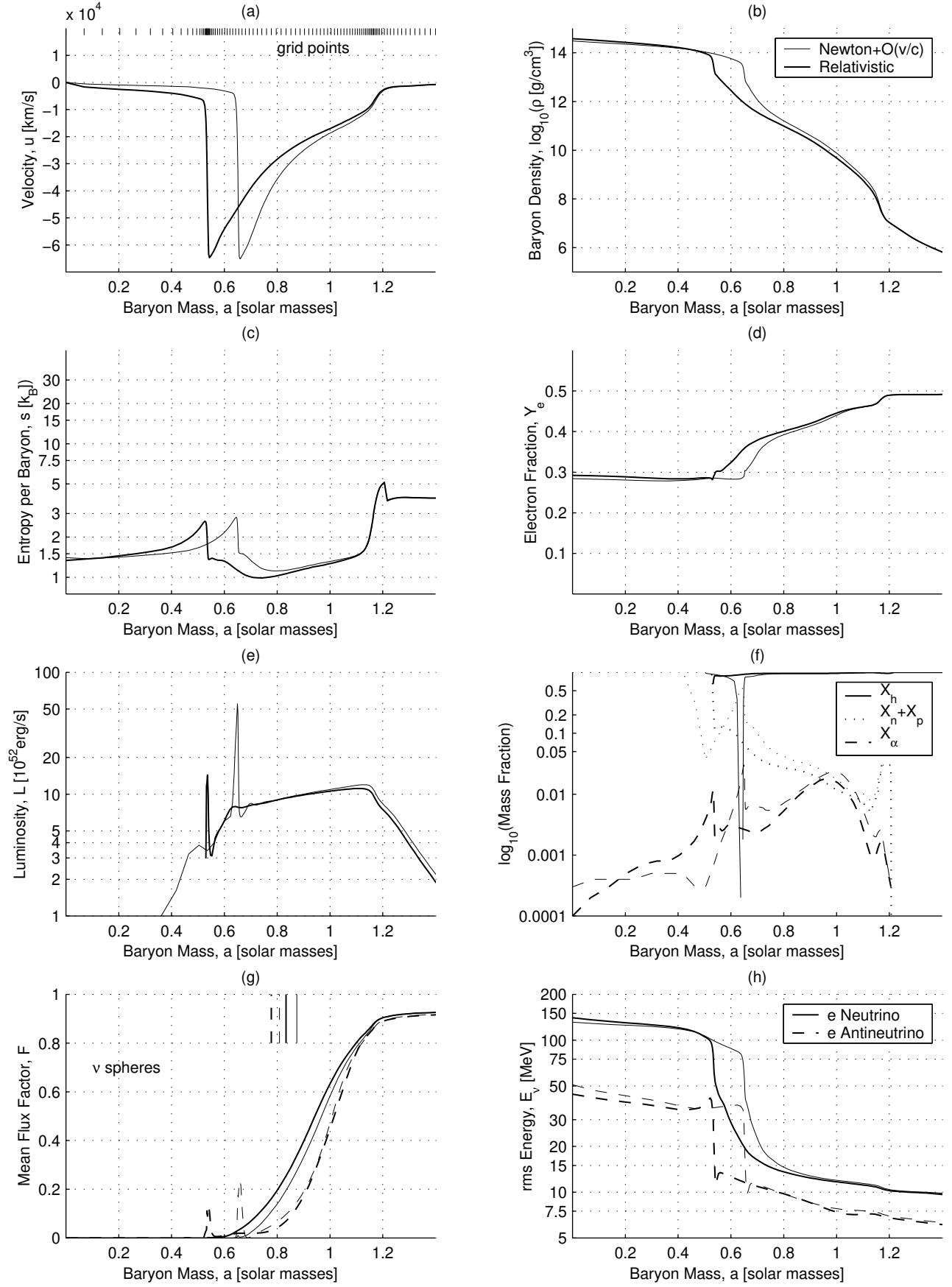


FIG. 1. Shock formation: Time slice at bounce.

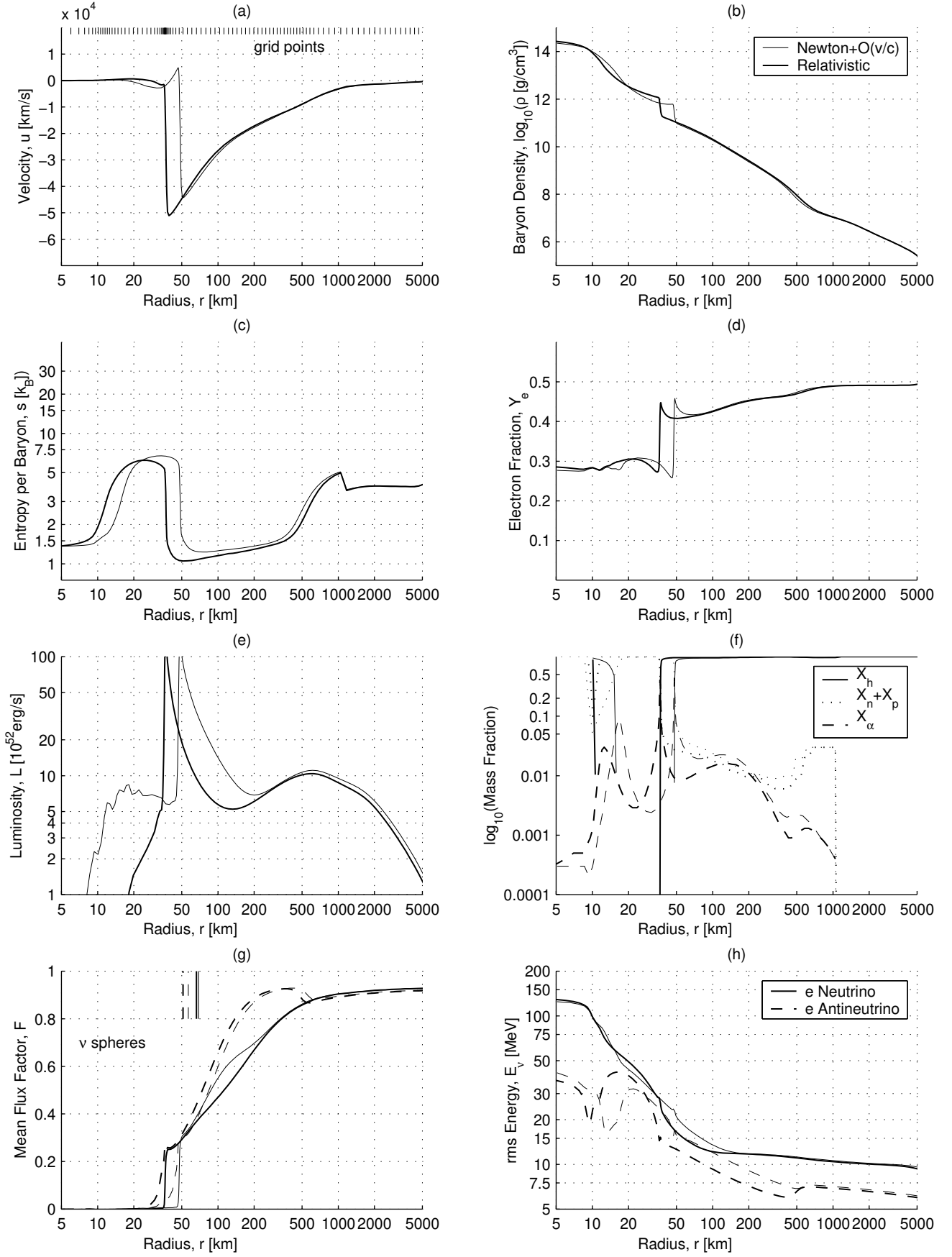


FIG. 2. Dissociation: Time slice at 1ms after bounce.

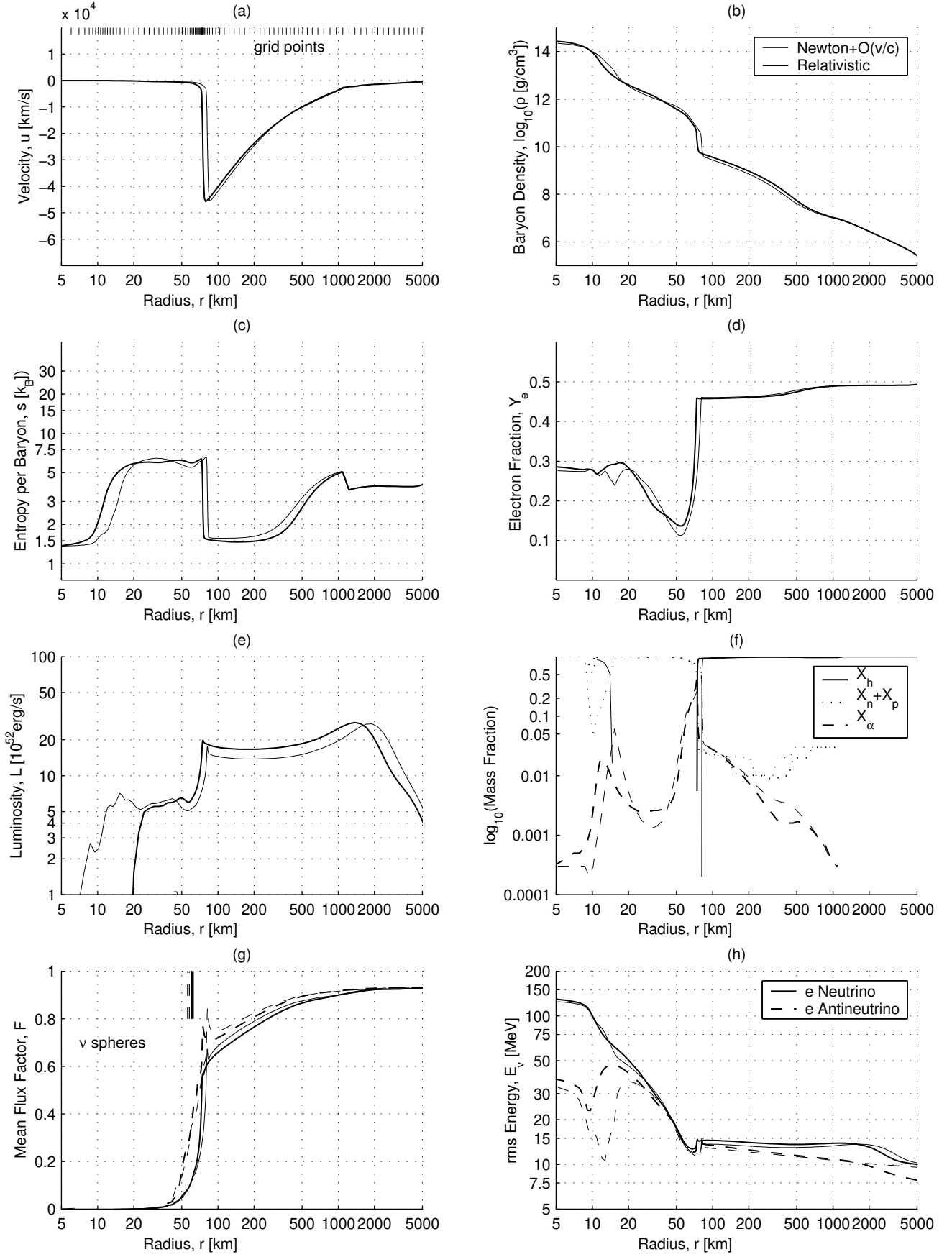


FIG. 3. Neutrino burst: Time slice at 10ms after bounce.

corresponding deleptonization behind the shock is dramatic in graph (d). The energy carried off with the neutrino burst completely drains the shock in both the NR and the GR cases. The pure accretion shock continues to propagate outwards as infalling material is dissociated and layered on the hot mantle (graph (a)). This stage is the definitive end of a “prompt”, i.e. purely hydrodynamic, explosion.

In the standard picture, the ensuing evolution is driven by electron neutrino heating. Electron flavor neutrinos are diffusing out of the hot core and created in the accreting and compactifying matter around the neutrinospheres. On their escape from the semi-transparent heating region, they deposit energy behind the shock by absorption on free nucleons. This situation is well established at 100ms after bounce, corresponding to Fig. (4). The accretion shock has passed the border of the original iron core. In graph (a), it has stalled at a radius of roughly 200km. The GR shock shows a smaller stall radius than the NR shock and the infall velocity behind the shock is about two times larger than in the NR case. The incomplete dissociation of the infalling silicon layer at the shock in graph (f) illustrates the weakening of the shock. Half the mass of the material right behind the shock remains bound in alpha particles. We additionally notice that all the heavy nuclei inside the shock radius have either been dissociated by compressional heating or been converted to bulk nuclear matter. This marks the end of the epoch during which there is an advantage in the NR case as far as binding energy of undissociated nuclei inside the shock radius is concerned. We see in graph (g) that the neutrino radiation becomes increasingly forward peaked outside of the neutrinospheres. There is an extended region between 50 and 200km where the neutrinos can deposit energy by absorption. In the interior part of this region, the net cooling region, this process is more than outweighed by neutrino emission of the infalling material via electron and positron capture while being compressed, heated, and layered onto the proto-neutron star. In the outer net heating region, however, electron flavor neutrino absorption just exceeds neutrino emission leading to comparatively small net heating. The heating can indirectly be observed in graph (c) where the entropy per baryon starts to increase behind the shock. We read from graph (g) that the neutrinospheres in the more compact and hotter GR core are at smaller radius. This leads to emission of neutrinos at higher rms energies (graph (h)). The discontinuity in the rms energies at the shock are due to the Doppler shift across it. All radiation quantities are calculated and plotted as measured by a comoving observer. This choice also leads to the luminosity step in graph (e), the infalling observer heading towards the center observes a higher luminosity than the observer almost at rest behind the shock. Although the GR luminosities in the heating region are up to 20% higher than in the NR case, the heating is not more effective in the GR case. The shocked material settles onto the proto-neutron star with a higher velocity in the deeper gravitational potential and therewith stays for a shorter time in the net heating region.

Finally, we show the situation at 500ms after bounce in Fig. (5). The shock in graph (a) has receded to 60km in the GR case and to 90km in the NR case. The accretion shock, sitting deep in the gravitational potential, experiences a high ram pressure from the infalling material. All nuclei are completely dissociated when they pass the shock (graph (f)). The infall velocities behind the shock are as large as 5000km/s in the NR simulation and almost double that in the GR simulation. This produces high accretion luminosities in the GR case, as shown in graph (e). Higher rms energies in the GR case are evident in graph (h), as expected from the deeper position of the neutrinospheres. The net heating is not very efficient on the infalling material, and the entropy per baryon increases only very slowly at $\sim 1.7k_B/100\text{ms}$. It reaches $20k_B$ in graph (c). Overall most features in the GR simulation are enhanced relative to the NR simulation, and the GR case exhibits a more compact structure in the proto-neutron star and its surroundings. The central density reached $5.15 \times 10^{14} \text{ g/cm}^3$ in graph (b).

The mass trajectories of shells containing $0.01 M_\odot$ as a function of time are shown for the relativistic simulation in Fig. (6). Note that the high velocities (steep gradients of mass traces) in the heating region can hardly be distinguished from the ten times larger infall velocities outside of the shock. As discussed above, mass elements are almost stopped at the shock front and do not directly fall onto the proto-neutron star surface, as might be inferred from Fig. (6). The shock position is drawn for both the GR and the NR simulation. The GR shock barely reaches 200 km, the NR shock reaches 230 km.

We close this description with two figures showing the temporal evolution of the GR radiation quantities. In Fig. (7) we show the neutrino luminosities at 500 km radius as a function of time. The electron luminosity is slowly rising during collapse and decreases as the core reaches maximal density. It remains suppressed for the $\sim 4\text{ms}$ the shock needs to propagate to the electron neutrinosphere. The most prominent feature is the electron neutrino burst, reaching $3.5 \times 10^{53} \text{ erg/s}$ at shock breakout, and declining afterwards. Graph (b) shows the luminosity spectra at 100ms after bounce, just before the shock starts to recede. Fig. (8) shows the long-term evolution with better resolution, sampled at a radius of 500 km. The maximum luminosities in the GR simulation are $3.9 \times 10^{52} \text{ erg/s}$, $3.6 \times 10^{52} \text{ erg/s}$, and $2.3 \times 10^{52} \text{ erg/s}$ for the electron neutrino, electron antineutrino, and μ, τ neutrinos respectively. This is roughly 10% more than the maximum luminosities reached (at different times) in the NR simulation. The GR results also show higher rms energies, but no qualitatively different features.

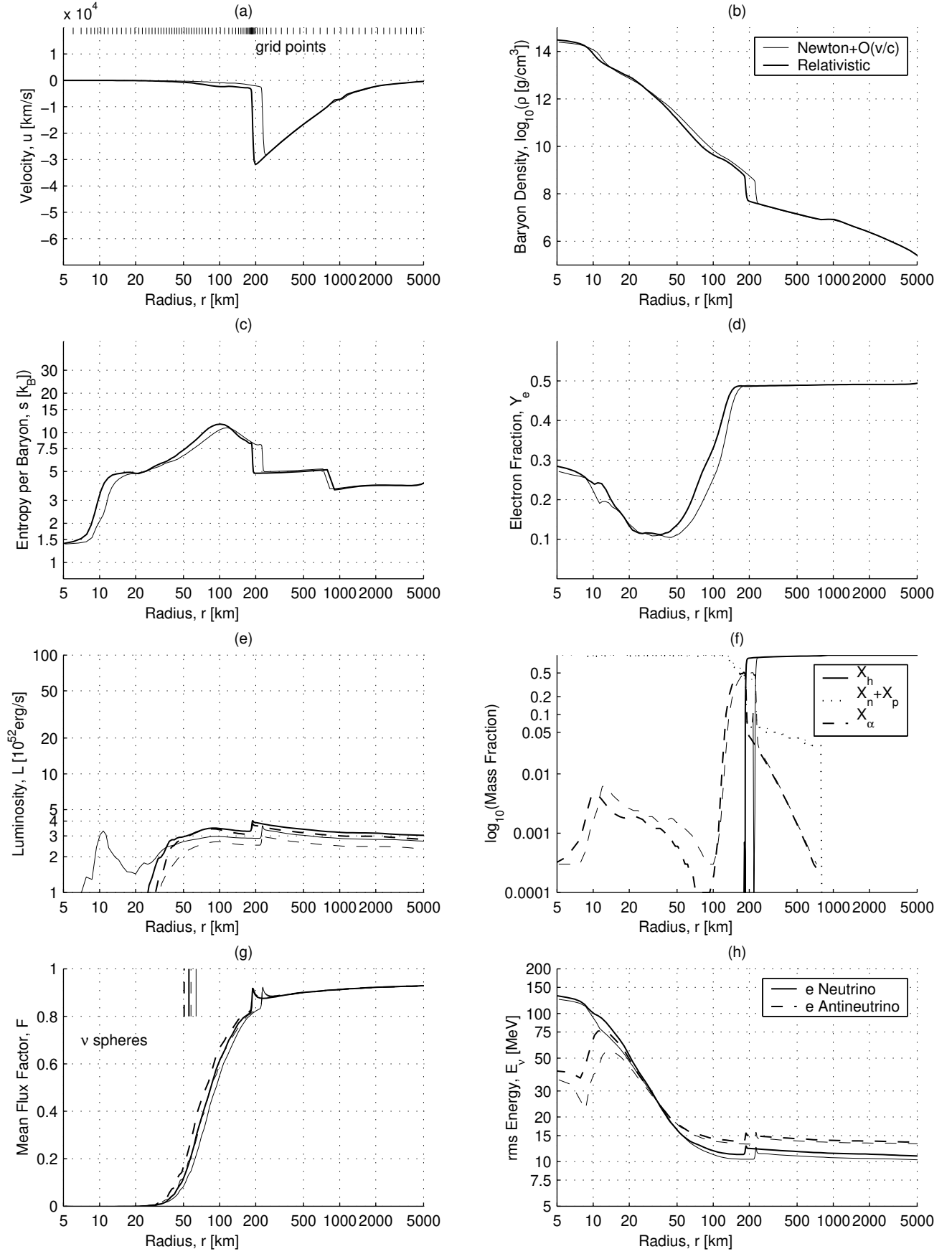


FIG. 4. Neutrino heating: Time slice at 100ms after bounce.

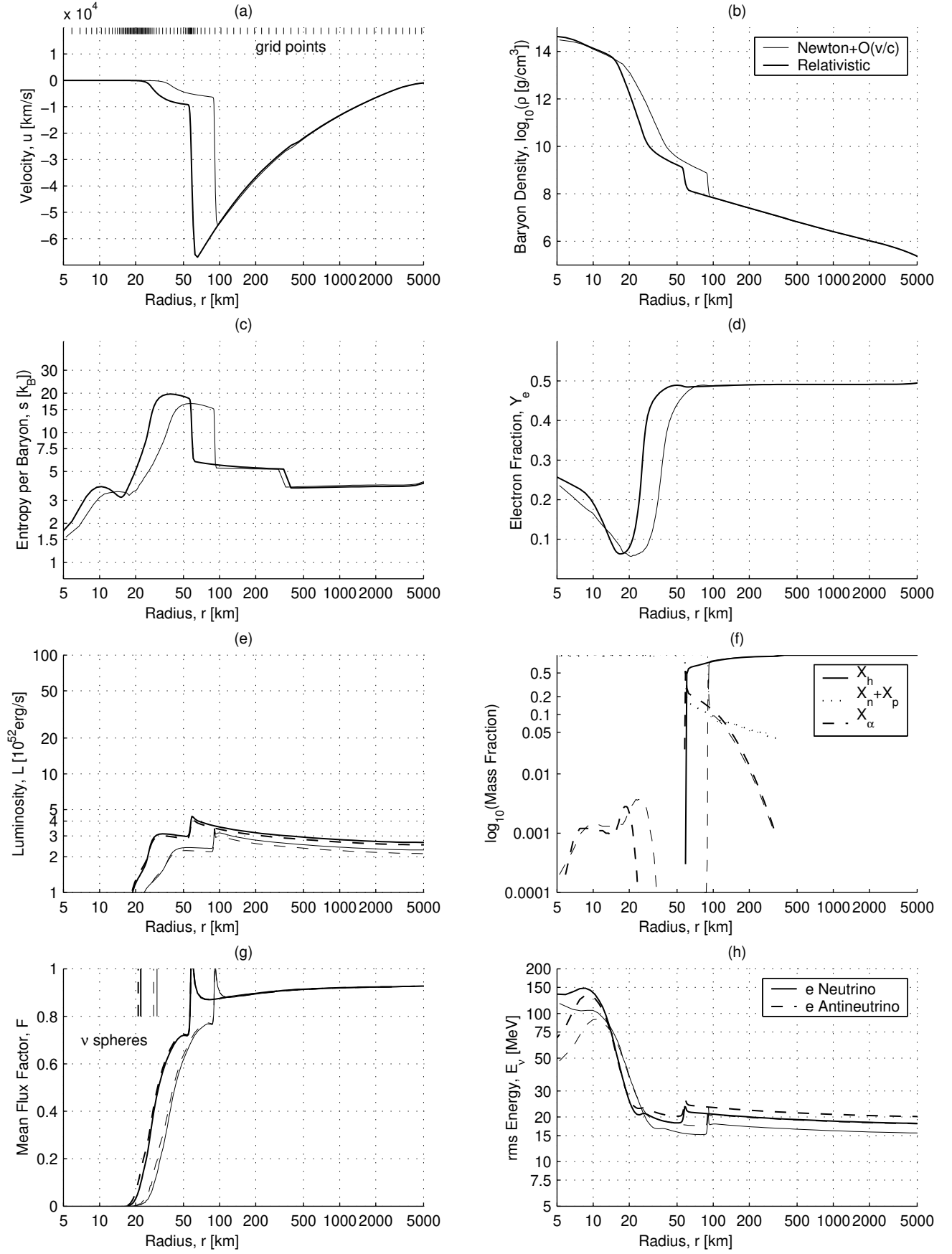


FIG. 5. Shock recession: Time slice at 500ms after bounce.

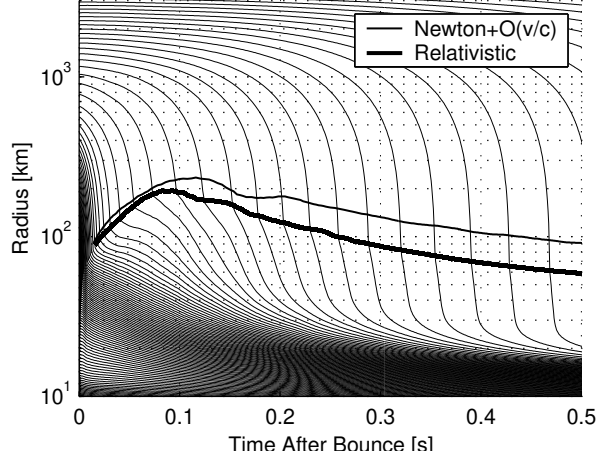


FIG. 6. Radial trajectories of equal mass shells ($0.01 M_{\odot}$) in the iron core and silicon layer.

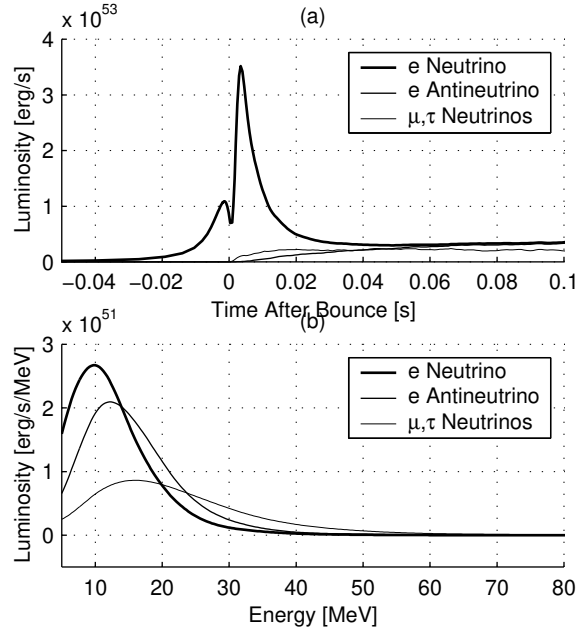


FIG. 7. (a) Neutrino luminosities before and after bounce showing the electron neutrino burst (sampled at 500 km radius and time shifted by $\Delta t = 500 \text{ km}/c$). (b) Neutrino energy spectra at a radius of 500 km, and 100ms after bounce.

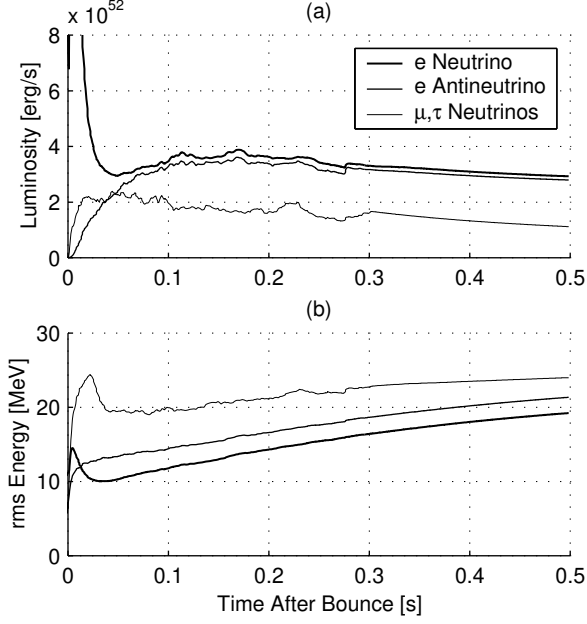


FIG. 8. Neutrino luminosities and rms energies versus time at a radius of 500 km.

IV. CONCLUSION AND OUTLOOK

We have completed the construction of a general relativistic radiation hydrodynamics code, AGILE-BOLTZTRAN, and simulated the spherically symmetric, general relativistic core collapse, bounce, and postbounce evolution of a $13 M_{\odot}$ progenitor. We investigate the confluence of (i) a deeper effective gravitational potential, (ii) a GR core hydrodynamic structure that acts as a more intense neutrino source, and (iii) an increased heating efficiency obtained from accurate three-flavor Boltzmann neutrino transport, in an attempt to model a spherically symmetric supernova.

For the following conclusions, we presuppose that neutrino heating plays an important role in supernovae and try to distinguish independent driving forces in the mechanism from dependent contributors. Independent forces are essentially unaffected by the postbounce evolution. This category contains the core luminosity as a part of the neutrino source, the deepness of the gravitational potential with its influence on neutrino propagation, and the absorption efficiency in the heating region. We distinguish this basic triple of emission, transport and absorption from secondary contributors, which themselves depend on the postbounce evolution. For example, the accretion-induced neutrino luminosities, the infall velocity in the heating region, and the motion of the shock and neutrinospheres are subject to a self-regulatory feedback in the spirit of Burrows and Goshy [34].

Focusing on the independent forces: (i) GR effects enhance the compression of the central region of the protoneutron star, which consequently becomes more compact. (ii) The more compact core in the GR simulation has a higher binding energy, which leads to larger core internal energies and temperatures. This in turn leads to higher core luminosities in all neutrino flavors (Bruenn et al. [41]). (iii) The solution of the exact Boltzmann equation for the neutrino transport reproduces accurately the angular distribution of the neutrino radiation field. An increased angular spread in the semi-transparent regime keeps the outstreaming neutrinos longer in the heating region and therefore increases the absorption efficiency with respect to the multigroup flux-limited diffusion approximation (Messer et al. [21], Yamada et al. [22]). (iv) The neutrinos in curved spacetime propagate on trajectories with nearly constant $\varepsilon = (\Gamma + U\mu)E$ and $b = R\sqrt{1 - \mu^2}/(\Gamma + U\mu)$, where μ and E are the neutrino propagation-angle cosine and energy measured by comoving observers.

We find that point (iv) is of little importance in our low-mass progenitor. The GR corrections for redshift and curvature between the neutrinospheres and the heating region do not exceed 3% until shock recession, and increase only later, when the neutrinospheres have receded to smaller radii. On the other hand, neither (ii) or (iii), nor their combination result in a successful supernova explosion for the investigated $13M_{\odot}$ progenitor. This stands in agreement with recent models that investigated a subset of these issues (Rampp and Janka [44], Mezzacappa et al. [43], Bruenn et al. [41]). In the failed explosion, the compact GR protoneutron star places the neutrinospheres at a smaller radius than in the NR case. The surrounding layers (heating region, shock radius) are also found at a smaller radius and

therewith deeper in the gravitational well. The accretion shock adjusts its equilibrium position according to the higher ram pressure of the infalling material, and the pressure of the hot shocked material in the gravitational potential. Equilibrium is achieved at higher infall velocities in the heating region and at higher accretion luminosities.

From the comparison between the NR and GR shock trajectories, we might be tempted to conclude that the chances for a vigorous explosion in the more realistic GR case are more pessimistic than in the NR case. We have, however, tried to separate the independent forces from the scenario-dependent ones to speculate on the outcome in a more realistic, explosive scenario:

Since supernovae by definition *explode*, the infall velocity behind the shock has to vanish at some point in the evolution. If this happens in the early heating phase, the shock and heating region in the GR and NR cases might still be at a larger radius and in a comparable gravitational potential, while the compact GR core delivers higher neutrino luminosities with higher rms energies. This situation could lead to a boost in the GR explosion energy relative to the NR case. Such a boost has actually been seen by Liebendörfer [42] in a simulation that led to an explosion because of incorrect nucleon isoenergetic scattering opacities. We would then conclude that, at least in low-mass progenitors with small redshifts, GR effects do not cause explosions, but eventually boost successful ones.

The modeling of core collapse supernovae has entered a new level of sophistication. General relativistic spherical models based on multigroup and multiflavor Boltzmann neutrino transport are now available. High-resolution simulations of the postbounce evolution with different progenitors will close remaining windows of uncertainty in spherically symmetric models. The focus will then sweep to a final open window: the uncertainties in the nuclear physics and neutrino interactions. A major revision in the equation of state (Shen et al. [51], see also Swesty et al. [38]), the neutrino-matter interactions (Burrows and Sawyer [52], Reddy et al. [53], Langanke and Martinez-Pinedo [54]), or neutrino oscillations might be the last chance for explosions in purely spherical models. Continued failure would suggest that rotation, convection, and/or magnetic fields are essential to successfully launch a supernova explosion.

ACKNOWLEDGMENTS

M.L. is supported by the National Science Foundation under contract AST-9877130 and, formerly, was supported by the Swiss National Science Foundation under contract 20-53798.98. A.M. is supported at the Oak Ridge National Laboratory, managed by UT-Battelle, LLC, for the U.S. Department of Energy under contract DE-AC05-00OR22725. F.-K.T. is supported in part by the Swiss National Science Foundation under contract 20-61822.00 and as a Visiting Distinguished Scientist at the Oak Ridge National Laboratory. O.E.B.M. is supported by funds from the Joint Institute for Heavy Ion Research and a Dept. of Energy PECASE award. W.R.H. is supported by NASA under contract NAG5-8405 and by funds from the Joint Institute for Heavy Ion Research. S.W.B. is supported by the NSF under contract 96-18423 and by NASA under contract NAG5-3903. Our simulations were carried out on the ORNL Physics Division Cray J90 and the National Energy Research Supercomputer Center Cray J90.

-
- [1] S. A. Colgate and R. H. White, *Astrophysical Journal* **143**, 626 (1966).
 - [2] M. M. May and R. H. White, *Computational Physics* **7**, 219 (1967).
 - [3] C. W. Misner and D. H. Sharp, *Physical Review* **136**, B571 (1964).
 - [4] R. W. Lindquist, *Annals of Physics* **37**, 487 (1966).
 - [5] J. R. Wilson, *Astrophysical Journal* **163**, 209 (1971).
 - [6] E. Baron, J. Cooperstein, and S. Kahana, *Nuclear Physics A* **440**, 744 (1985).
 - [7] J. Lattimer and F. D. Swesty, *Nuclear Physics A* **535**, 331 (1991).
 - [8] P. J. Schinder and S. L. Shapiro, *Astrophysical Journal Supplement Series* **50**, 23 (1982).
 - [9] S. W. Bruenn, *Astrophysical Journal Supplement Series* **58**, 771 (1985).
 - [10] A. Burrows and J. M. Lattimer, *Astrophysical Journal* **307**, 178 (1986).
 - [11] W. D. Arnett, *Astrophysical Journal* **218**, 815 (1977).
 - [12] R. L. Bowers and J. R. Wilson, *Astrophysical Journal Supplement Series* **50**, 115 (1982).
 - [13] E. S. Myra, S. A. Bludman, Y. Hoffman, I. Lichtenstadt, N. Sack, and K. A. Van Riper, *Astrophysical Journal* **318**, 744 (1987).
 - [14] S. W. Bruenn, *Astrophysical Journal* **340**, 955 (1989).
 - [15] S. W. Bruenn, *Astrophysical Journal* **341**, 385 (1989).
 - [16] J. R. Wilson and R. W. Mayle, *Physics Reports* **227**, 97 (1993).

- [17] H.-T. Janka, *Astronomy and Astrophysics* **256**, 452 (1992).
- [18] A. Mezzacappa and S. W. Bruenn, *Astrophysical Journal* **405**, 669 (1993).
- [19] A. Mezzacappa and S. W. Bruenn, *Astrophysical Journal* **405**, 637 (1993).
- [20] A. Mezzacappa and S. W. Bruenn, *Astrophysical Journal* **410**, 740 (1993).
- [21] O. E. B. Messer, A. Mezzacappa, S. W. Bruenn, and M. W. Guidry, *Astrophysical Journal* **507**, 353 (1998).
- [22] S. Yamada, H.-T. Janka, and H. Suzuki, *Astronomy and Astrophysics* **344**, 533 (1999).
- [23] S. W. Bruenn and T. Dineva, *Astrophysical Journal Letters* **458**, L71 (1996).
- [24] M. Herant, W. Benz, and S. A. Colgate, *Astrophysical Journal* **395**, 642 (1992).
- [25] D. S. Miller, J. R. Wilson, and R. W. Mayle, *Astrophysical Journal* **415**, 278 (1993).
- [26] M. Herant, W. Benz, R. W. Hix, C. L. Fryer, and S. A. Colgate, *Astrophysical Journal* **435**, 339 (1994).
- [27] A. Burrows, J. Hayes, and B. A. Fryxell, *Astrophysical Journal* **450**, 830 (1995).
- [28] H.-T. Janka and E. Müller, *Astronomy and Astrophysics* **306**, 167 (1996).
- [29] W. Keil, H.-T. Janka, and E. Müller, *Astrophysical Journal Letters* **473**, L111 (1996).
- [30] A. Mezzacappa, A. C. Calder, S. W. Bruenn, J. M. Blondin, M. W. Guidry, M. R. Strayer, and A. S. Umar, *Astrophysical Journal* **493**, 848 (1998).
- [31] A. Mezzacappa, A. C. Calder, S. W. Bruenn, J. M. Blondin, M. W. Guidry, M. R. Strayer, and A. S. Umar, *Astrophysical Journal* **495**, 911 (1998).
- [32] C. F. Fryer, *Astrophysical Journal* **522**, 413 (1999).
- [33] C. F. Fryer and A. Heger, *Astrophysical Journal* **541**, 1033 (2000).
- [34] A. Burrows and J. Goshy, *Astrophysical Journal Letters* **416**, L75 (1993).
- [35] H.-T. Janka, *Astronomy and Astrophysics*, submitted (2000).
- [36] E. Baron, J. Cooperstein, and S. Kahana, *Physical Review Letters* **55**, 126 (1985).
- [37] E. S. Myra and S. A. Bludman, *Astrophysical Journal* **340**, 384 (1989).
- [38] F. D. Swesty, J. M. Lattimer, and E. S. Myra, *Astrophysical Journal* **425**, 195 (1994).
- [39] I. Goldman and S. Nussinov, *Astrophysical Journal* **403**, 706 (1993).
- [40] K. De Nisco, S. W. Bruenn, and A. Mezzacappa, *American Astronomical Society Meeting*, 191, #39.10 (1997).
- [41] S. W. Bruenn, K. R. DeNisco, and A. Mezzacappa, *Astrophysical Journal*, submitted (2000).
- [42] M. Liebendörfer, Ph.D. thesis, University of Basel, (Basel, Switzerland, 2000).
- [43] A. Mezzacappa, M. Liebendörfer, O. E. B. Messer, R. W. Hix, F.-K. Thielemann, and S. W. Bruenn, *Physical Review Letters*, submitted (2000).
- [44] M. Rampp and H.-T. Janka, *Astrophysical Journal Letters* **539**, L33 (2000).
- [45] A. Burrows, T. Young, Ph. Pinto, R. Eastman, and T. A. Thompson, *Astrophysical Journal* **539**, 865 (2000).
- [46] K. Nomoto and M. Hashimoto, *Physics Reports* **163**, 13 (1988).
- [47] M. Liebendörfer, A. Mezzacappa, and F.-K. Thielemann, *Physical Review D*, submitted (2000).
- [48] M. Liebendörfer and F.-K. Thielemann, in *Nineteenth Texas Symposium on Relativistic Astrophysics*, edited by E. Aubourg, T. Montmerle, J. Paul, and P. Peter (Elsevier Science B. V., Amsterdam, 2000).
- [49] A. Mezzacappa and O. E. B. Messer, *Journal of Computational and Applied Mathematics* **109**, 281 (1998).
- [50] O. E. Messer, Ph.D. thesis, University of Tennessee, (Knoxville, USA, 2000).
- [51] H. Shen, H. Toki, K. Oyamatsu, and K. Sumiyoshi, *Nuclear Physics A* **637**, 435 (1998).
- [52] A. Burrows and R. F. Sawyer, *Physical Review C* **58**, 554 (1998).
- [53] S. Reddy, M. Prakash, J. M. Lattimer, and J. A. Pons, *Physical Review C* **59**, 2888 (1999).
- [54] K. H. Langanke and G. Martinez-Pinedo, *Nuclear Physics A* **673**, 481 (2000).